

Article

# A Novel Class of Functionally Tuneable Star-Shaped Molecules for Interaction with Multiple Proteins

Debashis Barik<sup>1</sup>, Geethanjali Anand<sup>1</sup>, Subba Rao Cheekatla<sup>1</sup>  and Mintu Porel<sup>1,2,\*</sup> 

<sup>1</sup> Department of Chemistry, Indian Institute of Technology Palakkad, Palakkad 678557, India; 202114005@smail.iitpkd.ac.in (D.B.); 202214001@smail.iitpkd.ac.in (G.A.); subbarao1@gmail.com (S.R.C.)

<sup>2</sup> Environmental Sciences and Sustainable Engineering Center, Indian Institute of Technology Palakkad, Palakkad 678557, India

\* Correspondence: mintu@iitpkd.ac.in

**Abstract:** Molecules with tuneable properties are well known for their applications in the material and bio-medical fields; nevertheless, the structural and functional tunability makes them more significant in diverse applications. Herein, we designed and synthesized a novel class of star-shaped molecules via incorporating two important functional groups, i.e., triazole and dithiocarbamate (DTC). The rationale behind selecting these two key functional groups is their diverse applications, e.g., DTC having applications for therapeutics, pesticides, and vulcanizing agents, and triazole having applications for anti-cancer, fungicides, anti-microbials, inhibitors, etc. The structure of the molecules was strategically designed in such a way that their overall structures are the same (central tertiary-amine and peripheral hydroxy groups), except the key functional group (DTC and triazole) in the respective molecules was different. Following synthesis and characterization, the influence of DTC and triazole groups on their bioactivity was compared via interacting with the most abundant proteins present in the blood, including serum albumin, trypsin, haemoglobin, and ribonuclease. From both the experimental and molecular docking studies, it was confirmed that the triazole molecule has a higher binding affinity towards these proteins as compared to the DTC molecule. In summary, two star-shaped DTC- and triazole-based molecules were synthesized and their bioactivity was compared via binding with blood plasma proteins.

**Keywords:** star-shaped molecule; dithiocarbamate; triazole; tuneable property; protein interaction



**Citation:** Barik, D.; Anand, G.; Cheekatla, S.R.; Porel, M. A Novel Class of Functionally Tuneable Star-Shaped Molecules for Interaction with Multiple Proteins. *Organics* **2023**, *4*, 219–231. <https://doi.org/10.3390/org4020018>

Academic Editor: Wim Dehaen

Received: 31 March 2023

Revised: 7 May 2023

Accepted: 12 May 2023

Published: 16 May 2023



**Copyright:** © 2023 by the authors. Licensee MDPI, Basel, Switzerland. This article is an open access article distributed under the terms and conditions of the Creative Commons Attribution (CC BY) license (<https://creativecommons.org/licenses/by/4.0/>).

## 1. Introduction

Molecules with structural diversity and tuneable properties uniquely qualifies them for a wide array of applications in material and bio-medical sciences. In order to increase their potential for different applications such as antibacterial, anticancer, antifungal, anti-trypansomatid, anti-inflammatory, and anti-leishmanial agents, as well as sensing and removal agents for various toxic pollutants including heavy metals, fungicides, insecticides, anions, nitroaromatics, and so on, molecules with tuneable functional groups will provide a great degree of versatility [1–13]. Therefore, the functional groups can be adjusted and the architecture can be tuned to alter how these molecules are used for various bio-medical and material applications [14,15]. A star-shaped molecule (SSM) has arms that radiate in a rail-like fashion from a central axle [16]. Due to the unique architecture and tuneable backbone of SSMs, they have a high degree of functionality, which in turn makes them versatile for various applications [17–19]. The higher surface area of SSMs is attributed to the large number of chains radiating from the core. In addition, this star-shaped architecture plays a crucial role in imparting a higher structural stability [20], which makes them an ideal candidate for diverse applications in various fields. Moreover, the incorporation of diverse functionalities in the tuneable backbone can also enhance the potential of SSMs for applications in material and bio-medical sciences [21]. As a

proof-of-principle, two important functionalities have been chosen for this study, namely dithiocarbamate (DTC) and triazole units. The influence of these functionalities on the properties of SSM was studied through taking an application in the bio-medical field [22].

Dithiocarbamates are a prominent class of compounds that play crucial roles in various fields including pharmaceuticals, chemical synthesis, peptide chemistry as an amino-protecting group, and as linkers [23–26]. Due to the strong nucleophilicity and redox properties of the sulphur atom in the DTC moiety, it has gathered significant importance among medicinal chemists as well [27–29]. The capacity of DTCs to create metal-complexes is also widely known. The anionic  $CS_2$  group effectively promotes the formation of complexes with transition metals, defining their potential as enzyme inhibitors. Moreover, their applications in the synthesis of important organic intermediates including thiourea, isothiocyanate, 2-imino-1,3-dithiolane, cyanamide, heterocyclic ring, and amides are notable. The presence of DTC moieties in various natural products having antitumor, fungicidal, herbicidal, and pesticide activity also throws light on the potential of DTC moieties in diverse fields of application [30–36]. On the other hand, triazoles are another important class of compounds, well-known for their biocompatibility and capability of forming hydrogen bonds, which can enhance solubility and be advantageous for binding to biomolecular targets. Some triazole based star-shaped scaffolds have shown importance in the design of solar cells. Additionally, star-shaped triazole systems act as drug-delivery vehicles and are useful in the synthesis of dendrimers which display better anticancer activity. The factors that contribute to this property of triazoles include low toxicity, chemical stability, and small size [37]. The smaller size of triazole makes it easy to diffuse through the biological membrane and, thus, allows it to interact with a broad range of biological molecules [38–42]. The chemical stability and resistance to degradation in the biological system make it a potential candidate as a drug with long-term effectiveness. Because of its reliability and biocompatibility, the triazole formation has become the gold standard of click-chemistry and found application in various fields such as drug design and development, proteomics, and DNA research. The simplicity with which azides and alkynes can be incorporated into molecules, as well as their relative stability under a variety of environments, accounts in part for the efficacy of this reaction. Azides and alkynes are essentially inert to the majority of organic and biological environments, molecular oxygen, water, and most frequent reaction conditions in organic synthesis. In short, the combination of these factors imparts a high degree of biocompatibility to the triazole moiety along with a wide range of applications. Due to these high impacts, DTC and triazole groups were focused in this work.

To find the druggable nature of a compound, and to find the safety and efficacy of a drug, drug–protein interaction studies are inevitable [43–47]. When we administer a drug molecule into our body, it interacts with various proteins of our body, including structural proteins, enzymes, receptors, and transporters. From these interactions, we can determine how the drug is absorbed, distributed, metabolized, and excreted (pharmacokinetics) as well as the working action of the drug (pharmacodynamics) inside the body. Therefore, bioactivity of the synthesized SSMs was explored through interacting with multiple plasma proteins. Taken together, considering the importance of dithiocarbamate, triazole, and star-shaped molecules, an effort was made here for the synthesis of novel DTC- and triazole-based star-shaped molecules. Moreover, the synthetic steps that has followed for the synthesis of T-SSM and DTC-SSM are highly selective, good yield and mild conditions. Furthermore, their bioactive properties were compared through binding with various proteins including serum albumins, trypsin, haemoglobin, and ribonuclease.

## 2. Materials and Methods

### 2.1. Chemicals

All chemical reagents used here were purchased from Sigma-Aldrich, Spectrochem, TCI, Merck, and Alfa Aesar. Bovine serum albumin (BSA), human serum albumin (HSA), trypsin, hemoglobin and ribonuclease were procured from Spectrochem and HiMedia.

All of the solvents, such as hexane, ethyl acetate, methanol, chloroform, acetonitrile, and PEG-200, were of analytical grade and were used as received without any further purification.

### 2.2. Synthesis of Tris(2-chloroethyl) Amine

Triethanol amine (1 mmol) was dissolved in 20 mL of  $\text{CHCl}_3$ , then it was treated slowly with thionyl chloride ( $\text{SOCl}_2$ ) (10 mmol) for 5 min. Followed by the addition of  $\text{SOCl}_2$ , dimethyl formamide (2 mmol) was added as a catalyst to the reaction mixture. The reaction was stirred for 3 h at 60 °C. The completion of the reaction was monitored using TLC in ethyl acetate and hexane (1:9). After the completion of the reaction, the reaction mixture was washed twice with saturated sodium bicarbonate ( $\text{NaHCO}_3$ ) solution and chloroform (1:1). The organic layer chloroform ( $\text{CHCl}_3$ ) was dried over anhydrous sodium sulphate and concentrated under reduced pressure. The product was purified using column chromatography (hexane and ethyl acetate). A greenish oil was isolated with 84% yield. The product was characterized using  $^1\text{H-NMR}$ ,  $^{13}\text{C-NMR}$  and LC-MS spectroscopic techniques.

### 2.3. Synthesis of Tris(2-azidoethyl) Amine

Tris (2-chloroethyl) amine (1 mmol) was treated with sodium azide (5 mmol) followed by the addition of 20 mL of water. The reaction mixture was stirred for 12 h at 60 °C. Completion of the reaction was monitored using TLC with ethyl acetate and hexane (2:8). After completion of the reaction, the reaction mixture was washed with ethyl acetate and water (1:1). The organic layer (ethyl acetate) was dried over sodium sulphate and concentrated under reduced pressure. A pure yellowish oil was obtained with 98% yield. The product was characterized using  $^1\text{H-NMR}$ ,  $^{13}\text{C-NMR}$  and LC-MS spectral data.

### 2.4. Synthesis of Alkyne Precursor

Ethanolamine (1 mmol) was treated with propargyl bromide (1.2 mmol) followed by the addition of base triethyl amine (1.5 mmol) in 20 mL acetonitrile ( $\text{CH}_3\text{CN}$ ) solvent. Then, the reaction mixture was stirred at room temperature for 1 h. Completion of the reaction was monitored using TLC with ethyl acetate and methanol (9:1). After the completion of the reaction, the solvent acetonitrile evaporated under reduced pressure. The product was washed with ethyl acetate and water (1:1). The organic layer (ethyl acetate) was dried over anhydrous sodium sulphate and concentrated under reduced pressure. The reaction mixture was purified via column chromatography (hexane and ethyl acetate). The product was accurately characterized using  $^1\text{HNMR}$  and LC-MS spectral data.

### 2.5. Synthesis of DTC-SSM

DTC-based star-shaped molecule (DTC-SSM) was synthesized by means of a three-component organic reaction. Diethanol amine (3 mmol) was treated with carbon sulfide ( $\text{CS}_2$ ) (6 mmol) followed by the addition of solvent polyethylene glycol-200 (2 mL) at room temperature. Then, the reaction mixture was stirred for 5 min for the synthesis of an in situ sulfide ion. Thereafter, tris(2-chloroethyl) amine (1 mmol) was slowly added and stirred for 30 min. The completion of the reaction was monitored using TLC with ethyl acetate and hexane (1:9). The final mechanism of the reaction was followed by the replacement of chlorine atom from tris(2-chloroethyl) amine with the in situ sulfide ion. After completion, the reaction mixture was washed with water and ethyl acetate (1:1). The organic layer (ethyl acetate) was dried over sodium sulphate and concentrated under reduced pressure. Thereafter, the reaction mixture was purified using HPLC (High performance liquid chromatography) with 60% acetonitrile and water. The product was characterized using  $^1\text{H-NMR}$ ,  $^{13}\text{C-NMR}$ , FT-IR and LC-MS, and HRMS data.

### 2.6. Synthesis of T-SSM

Alkyne precursor (Scheme S3) (3 mmol) was added to tri-azide (S2) (1 mmol) followed by the addition of 5 mL of methanol. Thereafter, an aqueous solution of sodium-L-ascorbate

(1.2 mmol in 2.5 mL water) was added to the reaction mixture and stirred for five minutes. Then, aqueous solution of copper sulphate pentahydrate (0.2 mmol in 2.5 mL water) was added to the reaction mixture. The reaction mixture was stirred for 1 h at room temperature. Completion of the reaction was monitored by TLC with ethyl acetate and methanol (9:1). The reaction mixture was filtered to remove the sodium-L-ascorbate. Following filtration, the reaction mixture was concentrated under reduced pressure. Then, the reaction mixture was washed with water and ethyl acetate (1:1). The product was obtained in the water layer and concentrated under reduced pressure. The product was characterized using  $^1\text{H-NMR}$ ,  $^{13}\text{C-NMR}$ , FT-IR and LC-MS data.

### 2.7. Interaction Study of Molecules and Proteins

The protein interaction study of molecules was performed with Perkin Elmer (Waltham, MA, USA) FL 6500 at 25 °C. An excitation wavelength of 280 nm and a slit width of 5 nm were set for all of the protein binding studies in the spectrofluorometer. Then, 10  $\mu\text{M}$  solutions of proteins (BSA, HSA, ribonuclease, hemoglobin and trypsin) were created in pH 7.4 phosphate buffer. A 2 mM stock solution of DTC-SSM and T-SSM were prepared in DMSO and water, respectively. The titration studies were carried out by adding 2  $\mu\text{M}$  to 100  $\mu\text{M}$  concentrations of molecules. The binding constant was calculated by plotting  $I_0/I$  and the molecule concentration in the Stern–Volmer plot.

### 2.8. LC-MS, FT-IR and NMR

The LC-MS experiments were performed using a Shimadzu LC-MS-8045 with a Sprite TARGA C18 column (40  $\times$  2.1 mm, 5  $\mu\text{m}$ ), monitoring at 210 and 254 nm with a positive mode for mass detection. The compounds were eluted with a gradient of 0–100% (acetonitrile and water) with 0.7 mL/min over 15 min. FT-IR characterization was performed with Shimadzu IR Tracer 100 using the KBr pellet method. Mass spectra (HRMS) were recorded under positive ion electrospray ionization (ESI, Q-TOF) mode.  $^1\text{H NMR}$  were recorded on Bruker AV III 500 MHz and the data were analyzed via MestReNova (version 8.1.1).  $^1\text{H NMR}$  of tris-azide precursor, 500 MHz in  $\text{CDCl}_3$ :  $\delta$  (ppm) 2.78–2.81 (t, 6H,  $J = 5$  Hz), 3.35–3.37 (t, 6H,  $J = 5$  Hz).  $^1\text{H NMR}$  of alkyne precursor, 400 MHz in  $\text{CDCl}_3$ :  $\delta$  (ppm) 2.64–2.65 (t, 1H), 2.67–2.69 (t, 4H,  $J = 4$  Hz), 3.48 (d, 2H), 3.56–3.58 (t, 4H,  $J = 4$  Hz).  $^1\text{H NMR}$  of DTC-SSM, 500 MHz in  $\text{DMSO-}d_6$ :  $\delta$  (ppm) 2.80–2.83 (t, 6H,  $J = 5$  Hz), 3.66–3.70 (m, 12H), 3.88–3.91 (t, 6H,  $J = 5$  Hz), 4.08–4.10 (t, 6H,  $J = 5$  Hz), 4.85–4.87 (t, 3H,  $J = 5$  Hz), 5.01–5.03 (t, 3H,  $J = 5$  Hz).  $^1\text{H NMR}$  of T-SSM, 400 MHz in  $\text{D}_2\text{O}$ :  $\delta$  (ppm) 2.70 (s, 12H), 2.96 (s, 12H), 3.27 (s, 6H), 3.94 (s, 6H), 4.27 (s, 6H), 7.72 (s, 3H).  $^{13}\text{C-NMR}$  of tris-chloro precursor **2**, 400 MHz in  $\text{CDCl}_3$ :  $\delta$  (ppm): 42.06, 56.77, 76.71–77.35.  $^{13}\text{C-NMR}$  of tris-azide precursor **3**, 400 MHz in  $\text{CDCl}_3$ :  $\delta$  (ppm): 49.61, 53.93–54.35, 76.82–77.45.  $^{13}\text{C-NMR}$  (500 MHz) of DTC-SSM in  $\text{DMSO-}d_6$ :  $\delta$  (ppm): 34.747, 39.475, 40.476, 52.511, 56.414, 57.979, 58.514, 79.645, 196.302.  $^{13}\text{C-NMR}$  (400 MHz) of T-SSM in  $\text{D}_2\text{O}$ :  $\delta$  (ppm): 76.37, 77.25, 79.06, 99.99, 120.95, 123.66. HRMS data of DTC-SSM: calculated mass: 639.1400 Da; observed mass: 639.1507 Da. HRMS data of T-SSM: calculated mass: 654.4100 Da; observed mass: 654.4157 Da.

### 2.9. Molecular Docking Studies

Molecular docking studies were carried out using Auto Dock Vina [29] and Perl script for integration executables. The protein structure was collected from the protein bank for BSA (4F5V, chain A), HSA (1BM0, chain A), trypsin (1TRN, chain A), hemoglobin (4HHB, chain A) and ribonuclease A (2G8Q, chain A) <http://www.rcsb.org> accessed on 12 May 2022. The Autodock tool [48] was used for the addition of hydrogen atoms and Gasteiger charges. The grid boxes used had the following sizes: for BSA (X: 34.167, Y: 24.806, Z: 41.472), centred at (62, 80, 74); HSA (X: 29.607, Y: 31.782, Z: 23.488), centred at (60, 60, 60); trypsin (X: 2.494, Y: 7.537, Z: 21.194), centred at (42, 36, 52); hemoglobin (X: 14.422, Y: 67.713, Z: 4.181), centred at (100, 90, 110); and ribonuclease A (X: 5.325, Y: -26.182, Z: -15.471), centred at (84, 72, 116). The ligand structure was minimized by Argus lab (4.0.1) [49], The docked

structure was visualized by Pymol and the interaction of amino acid residues with the ligand was determined via Discovery studio [50].

### 3. Results and Discussion

#### 3.1. Design, Synthesis, and Characterization

The synthesis of the two star-shaped molecules (SSMs) was designed in such a way that the architecture of the molecules was same but the functional group in the backbone was different—dithiocarbamate in one case and triazole in the other. Moreover, followed by the incorporation of dithiocarbamate and triazole functional groups, the focus shifted towards the overall construction of molecules. For example, the tertiary amine in the central part of molecules facilitates different chemical properties, such as pH sensitivity, basicity and nucleophilicity and the hydroxyl group in the peripheral part facilitates water solubility and various biological processes.

##### 3.1.1. Synthesis of the Tris-Chloro, Tris-Azide and Alkyne Precursors

The synthesis starts from a readily available commercial material such as triethanol amine (1, Scheme 1). Triethanol amine was dissolved in chloroform ( $\text{CHCl}_3$ ) followed by reacting with thionyl chloride in the presence of dimethyl formamide (DMF), which acts as a catalyst which produces the tris(2-chloroethyl) amine (2, Scheme 1). Followed by the completion of the reaction, the reaction mixture was quenched with saturated sodium bicarbonate solution. Sodium bicarbonate solution was used to neutralize the hydrochloric acid (HCl) produced by the reaction mixture. After the neutralization of the reaction, the reaction mixture was washed with water and chloroform. The product was extracted with chloroform and dried under reduced pressure. Furthermore, the salt produced in the reaction mixture was dissolved in the aqueous solvent. The reaction mixture was purified by column chromatography and then taken to the next step. Tris(2-chloroethyl) amine was treated with sodium azide and the reaction mixture was refluxed at  $60\text{ }^\circ\text{C}$  for 12 h to yield tris(2-azidoethyl) amine (3, Scheme 1). Then, the reaction mixture was extracted two times with ethyl acetate and water (1:1), and the product was obtained in the ethyl acetate layer. Here, the mechanism of the reaction followed the nucleophilic substitution of chloride functional groups of Tris(2-chloroethyl) amine with an azide ( $\text{N}_3^-$ ) ion produced from the sodium azide salt. Compounds 2 and 3 (Scheme 1) were the primary precursors for the synthesis of DTC-SSM and T-SSM, respectively. An alkyne precursor (5, Scheme 1) was synthesized for the synthesis of T-SSM. The synthesis of alkyne precursor was started using a commercial and readily available starting material such as diethanol amine. Diethanol amine was reacted with propargyl bromide in the presence of triethyl amine in acetonitrile (ACN) to yield 2,2'-(prop-2-yn-1-ylazanediyl) bis(ethan-1-ol) (5, Scheme 1). The mechanism of the reaction followed the nucleophilic attack of the secondary nitrogen center of diethanol amine with the propargyl bromide. Followed by the completion of the reaction, the solvent was concentrated under reduced pressure and washed with water and ethyl acetate (1:1). The product was obtained in the ethyl acetate layer and purified using column chromatography. All of the synthesized compounds were characterized using  $^1\text{H}$  NMR,  $^{13}\text{C}$ -NMR, and LC-MS data (Figures 1i–iii and S1–S5).  $^1\text{H}$  NMR of tris-chloro precursor, 500 MHz in  $\text{CDCl}_3$ :  $\delta$  (ppm) 2.97–2.99 (t, 6H,  $J = 5\text{ Hz}$ ), 3.50–3.53 (t, 6H,  $J = 5\text{ Hz}$ ).

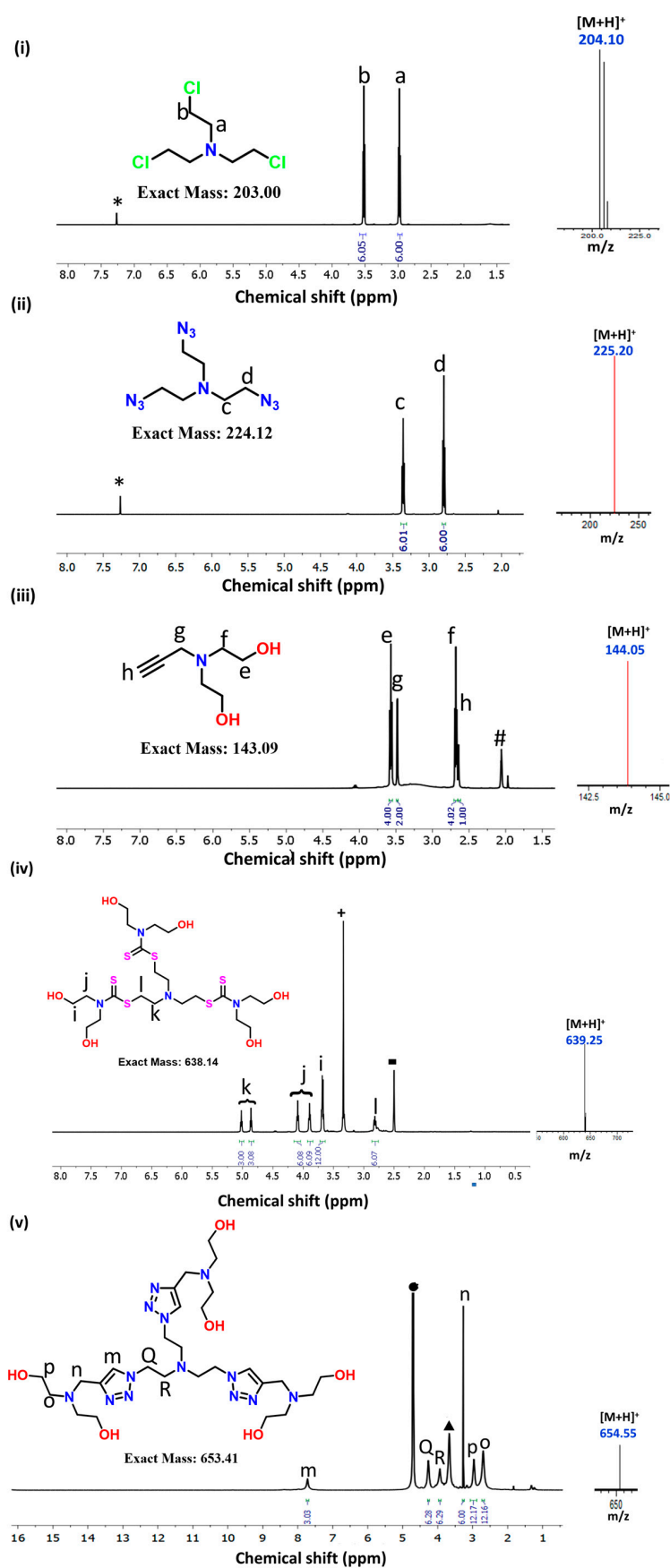


Figure 1. Characterization by means of <sup>1</sup>H-NMR (left) and mass spectrometry (right) of (i) tris(2-

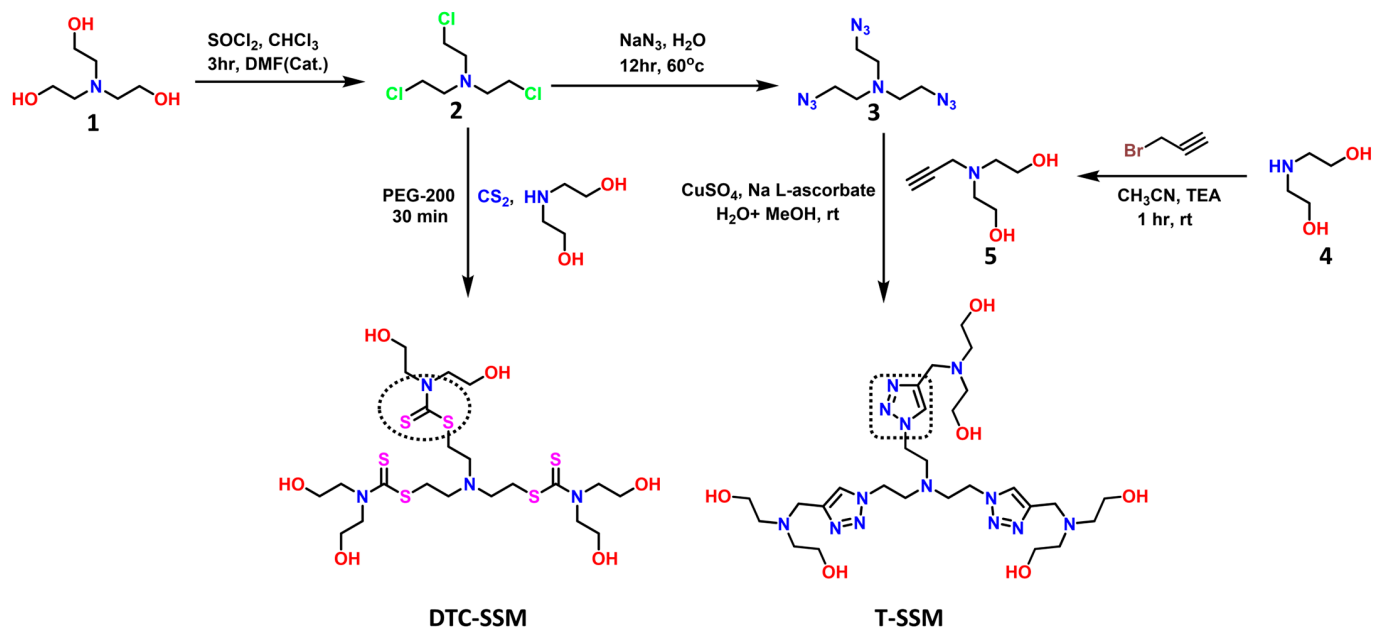
chloroethyl) amine (calculated  $[M+H]^+$ : 204.00 Da, observed  $[M+H]^+$ : 204.10 Da); (ii) tris(2-azidoethyl) amine (calculated  $[M+H]^+$ : 225.12 Da, observed  $[M+H]^+$ : 225.20 Da), (iii) alkyne precursor (calculated  $[M+H]^+$ : 144.05 Da and calculated  $[M+H]^+$ : 144.05 Da), (iv) DTC-SSM (calculated  $[M+H]^+$ : 639.14 Da, observed  $[M+H]^+$ : 639.25 Da) and (v) T-SSM (calculated  $[M+H]^+$ : 654.41 Da, observed  $[M+H]^+$ : 654.55 Da); ‘\*’, ‘#’, ‘■’, ‘●’, ‘+’, represent residual proton signals of the  $CDCl_3$ , acetone, DMSO,  $D_2O$ , and  $H_2O$ , respectively. ‘▲’ represents the exchanged out hydroxy protons of T-SSM in  $D_2O$  solvent.

### 3.1.2. Synthesis of DTC-Based Star-Shaped Molecules (DTC-SSM)

DTC-based star-shaped molecules (DTC-SSM) were synthesized by means of a three-component organic reaction. Firstly, diethanol amine was treated with carbon disulfide ( $CS_2$ ) followed by the addition of tris(2-chloroethyl) amine (2, Scheme 1). Then, the reaction mixture was stirred for 30 min at room temperature. The mechanism of the reaction was carried out via a three-component organic reaction. The advantages of this reaction are that it is highly selective, has mild reaction conditions and high yields. In this reaction, very mild HCl is produced which can be removed by means of the solvent extraction process. First, the reactive secondary nitrogen functional group of diethanol amine will react with the  $CS_2$  functional group, and results in the synthesis of an in situ sulfide ion. Furthermore, the sulfide ion will undergo nucleophilic substitution into the chlorine functional groups of tris(2-chloroethyl) amine, resulting in the synthesis of DTC-SSM. After the completion of the reaction, the reaction mixture was washed with water and ethyl acetate (1:1) and the product (DTC-SSM, Scheme 1) was obtained in the ethyl acetate layer. Furthermore, the ethyl acetate was evaporated under reduced pressure and a thick yellowish liquid was obtained in the round bottom flask with 88% yield. After the synthesis, the reaction mixture was purified by means of HPLC (high performance liquid chromatography) with 60% acetonitrile and water. The pure product (DTC-SSM) was characterized using  $^1H$  NMR, LC-MS (liquid chromatography coupled with mass spectrometry), infrared spectroscopy (FT-IR),  $^{13}C$ -NMR and HRMS. (Figures 1iv and S6–S9).

### 3.1.3. Synthesis of Triazole Based Star-Shaped Molecules (T-SSM)

The synthesis of triazole-based molecules (T-SSM) was carried out using the well-known copper-catalyzed azide-alkyne cycloaddition reaction (CuAAC). The advantages of the click reaction are its high yield, mild reaction conditions, orthogonal nature and versatility. Tris(2-azidoethyl) amine was reacted with alkyne precursor in the presence of  $CuSO_4 \cdot 5H_2O$  and sodium-L-ascorbate delivered the star-shaped T-SSM framework (Scheme 1). Followed by the completion of the reaction, the reaction mixture was filtered to remove the sodium-L-ascorbate and evaporated under reduced pressure. Thereafter, the reaction mixture was washed with water and ethyl acetate, and the product (T-SSM, Scheme 1) was obtained in the water layer. The synthesized product was characterized using  $^1H$  NMR, LC-MS (liquid chromatography coupled with mass spectrometry),  $^{13}C$ -NMR, infrared spectroscopy (FT-IR) and HRMS data (Figures 1v and S10–S13).



**Scheme 1.** Synthetic strategy for DTC- and triazole-based star-shaped molecules.

### 3.2. Comparison of Properties between DTC-SSM and T-SSM

The tunability of macromolecular properties is an essential criterion to make a material applicable in diverse fields. DTC-SSM and T-SSM showed differences in their properties based on their functional groups. The DTC-SSM showed more hydrophobicity than T-SSM (Figure 2), because DTC contained a sulfur group, which is larger in size, making it more hydrophobic [51]. Similarly, T-SSM is more hydrophilic in nature as compared to DTC-SSM due to the nitrogen atom in its triazole rings. This hydrophobic/hydrophilic property was confirmed by means of reversed-phase high-performance liquid chromatograms (RP-HPLC) of T-SSM and DTC-SSM (Figure 2).

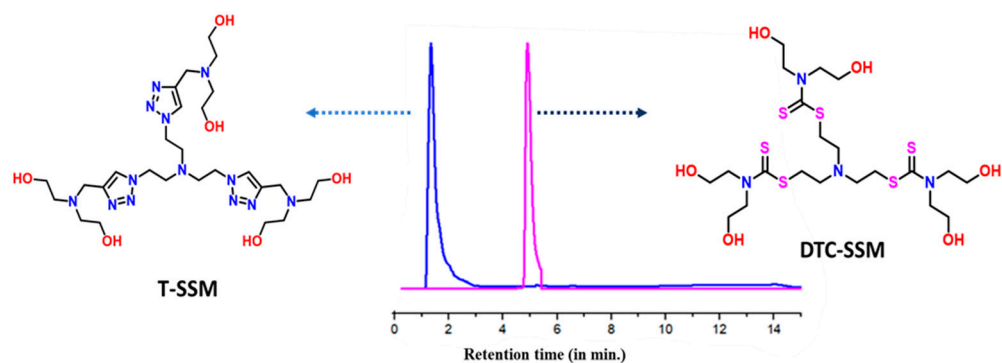


**Figure 2.** Reverse-phase high-performance liquid chromatography (RP-HPLC) traces of two molecules (T-SSM and DTC-SSM). Acetonitrile and water with 0.1% formic acid were used as the eluting solvent. The compounds were eluted for 15 min in 5–95% acetonitrile in water.

### 3.3. Protein Binding Studies of Molecules

Protein binding is a primary test for a molecule to prove its druggable behavior. Hence, to understand the druggable behavior of the compounds, the protein binding study of DTC-SSM and T-SSM was carried out with five essential proteins present in the blood, including human serum albumin (HSA), bovine serum albumin (BSA), hemoglobin, ribonuclease A and trypsin (Figures 3 and S14–S21). Generally, the proteins are fluorescent in behavior due to the presence of tryptophan and tyrosine residues. So, by taking advantage of the fluorescent nature of the proteins, the binding studies were carried out using the spec-

trofluorometer. The quenching of the fluorescence intensity of the proteins by adding both of the molecules revealed the interaction between them. From the fluorescence titration studies, it was observed that T-SSM has high binding affinity to all of the blood proteins as compared to DTC-SSM (Table 1). Furthermore, to understand the molecular-level interaction between the molecules and proteins, a molecular docking study was performed (Figures 4, 5 and S32–S41). From the study, it was observed that the triazole rings in the T-SSM help to provide an extra pi–pi interaction with the proteins, which greatly favor high binding interactions with proteins as compared to DTC-SSM. In addition, synchronous fluorescence titrations of these proteins were carried out to understand the changes happening in the microenvironment of the amino acid residues, tryptophan (trp) and tyrosine (tyr), as they are responsible for the intrinsic fluorescence of these proteins. If  $\Delta\lambda = 60$  nm has a higher decrement to the fluorescence emission intensity than that of  $\Delta\lambda = 15$  nm, then it indicates a higher degree of interaction of the molecules with tryptophan residues than the tyrosine residues [52]. To study the interactions of the T-SSM and DTC-SSM with serum proteins, synchronous fluorescence titrations were performed at  $\Delta\lambda = 15$  nm and  $\Delta\lambda = 60$  nm. Although the interaction occurred in both of the sites, a higher decrease in fluorescence intensity was observed for  $\Delta\lambda = 60$  nm when compared to  $\Delta\lambda = 15$  nm for all of the proteins (BSA, HSA, Hemoglobin, and trypsin), excluding ribonuclease A (Figures S22–S29). In the case of ribonuclease A, a higher decrement in fluorescence intensity was observed for  $\Delta\lambda = 15$ , which indicates the both of the molecules interacted more with the tyrosine amino acid residues of ribonuclease A (Figures S30 and S31).

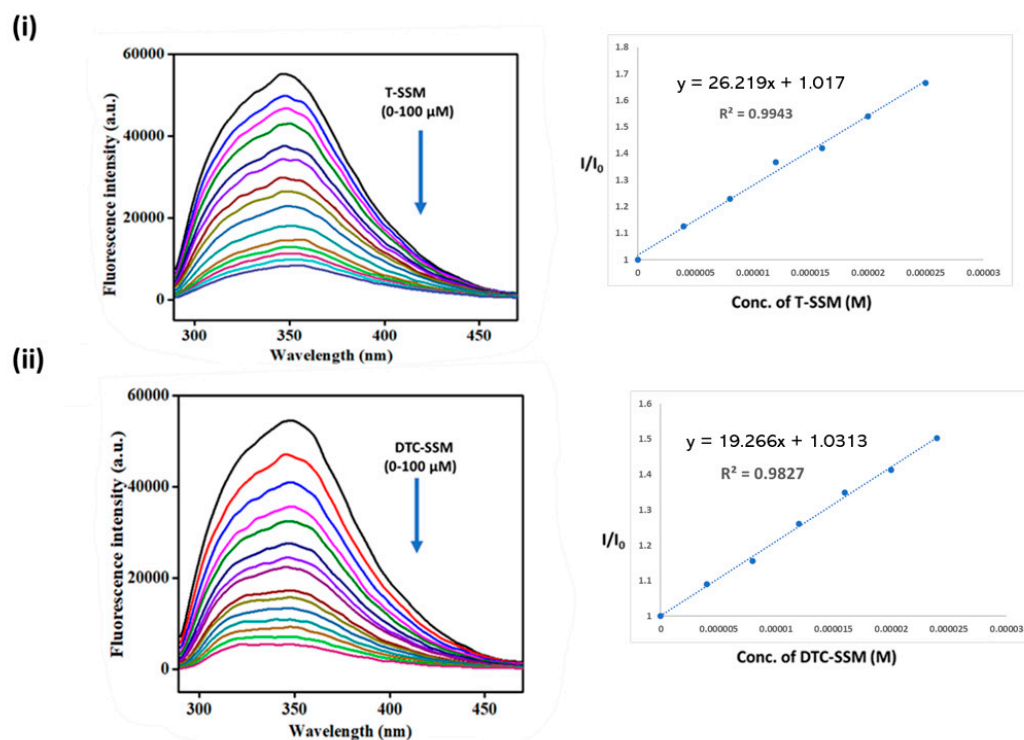


**Figure 3.** Fluorescence quenching of HSA (human serum albumin) protein by (i) triazole-based molecules and (ii) DTC-based molecules, at an excitation wavelength of 280 nm. To 10 μM protein solution in phosphate buffer (pH 7.4), 2–100 μM molecule solutions were added at 25 °C. Inset: Stern–Volmer Plot;  $I_0$  and  $I$  are the fluorescence intensity at 0 μM and the given concentration of the molecules, respectively, and the slope is considered as the binding constant.



#### 4. Conclusions

Herein, a strategy has been reported for the synthesis of star-shaped molecules with a tunable functional group. For the proof of principle, the tunability in the backbone was achieved with two important functional groups, i.e., triazole and dithiocarbamate. Furthermore, the synthetic strategies followed for the synthesis of DTC-SSM and T-SSM are highly selective, high-yield, have mild reaction conditions, versatile and orthogonal in nature. Moreover, the druggable nature of these compounds was studied by binding with the five important proteins in the blood, including BSA, HSA, trypsin, hemoglobin and ribonuclease. It was observed that both the molecules bind with the proteins significantly. Interestingly, triazole-based SSM showed higher binding to the proteins as compared to DTC-SSM. The molecular docking study supports the experimental results and validates that nitrogen containing a triazole moiety helps for provide an extra pi–pi interaction with the proteins. Due to the enormous application potential of star-shaped molecules, we are currently focusing on the development of novel strategies for the design of star-shaped molecule with a tunable side chain and functional groups. Overall, this study provides insights on the importance of shape and tunability in functional groups in star-shaped molecules for various biological and material applications. This kind of scaffold acts as a key synthon for various targets and might provide a valuable direction for the design of dendrimers as well as in host–guest supramolecules.

**Supplementary Materials:** The following supporting information can be downloaded at: <https://www.mdpi.com/article/10.3390/org4020018/s1>, Figures S1 and S2. Characterization of tri chloro precursor; Figures S3 and S4. Characterization of tri azide; Figure S5. Characterization of alkyne precursor; Figures S6–S9. Characterization of DTC-SSM; Figures S10–S13. Characterization of T-SSM; Figures S14–S21. Protein binding studies of molecules with proteins; Figures S22–S31. Synchronous spectra of protein binding and respective molecules; Figures S32–S41. Molecular docking of the interaction between proteins and molecules; Table S1. Binding energy of molecules and proteins from docking studies. Scheme S1: Synthesis of tri-chloro precursor; Scheme S2: Synthesis of tri-azide precursor; Scheme S3: Synthesis of alkyne precursor; Scheme S4: Synthesis of DTC-SSM; Scheme S5: Synthesis of T-SSM.

**Author Contributions:** M.P. conceptualized the design of star-shaped molecule with tunable properties; D.B. and G.A. carried out the synthesis, purification and characterization. D.B. and G.A. carried out all of the protein binding studies. D.B., G.A., S.R.C. and M.P. analyzed the data and D.B., G.A. and M.P. wrote the paper. All authors have read and agreed to the published version of the manuscript.

**Funding:** This research was funded by the Indian Institute of Technology Palakkad, India; the Ramanujan Fellowship (SB/S2/RJN-145/2017), Science and Engineering Research Board, Department of Science and Technology, India; the Core Research Grant (CRG/2019/002495), Science and Engineering Research Board, Department of Science and Technology, India; and the Scheme for Transformational and Advanced Research in Sciences (MoE/STARS-1/293), Ministry of Education and Technology, India.

**Data Availability Statement:** May be available upon request from the corresponding author.

**Acknowledgments:** We sincerely acknowledge the Central Instrumentation Facility (CIF) at the Indian Institute of Technology Palakkad and SAIF IIT Madras, India.

**Conflicts of Interest:** The authors declare no conflict of interest.

#### References

1. Baghershiroudi, M.; Safa, K.D.; Adibkia, K.; Lotfipour, F. Synthesis and antibacterial evaluation of new sulfanyl tetrazole derivatives bearing piperidine dithiocarbamate moiety. *Synth. Commun.* **2018**, *48*, 323–328. [[CrossRef](#)]
2. Laskar, S.; Sánchez-Sánchez, L.; Flores, S.M.; López-Muñoz, H.; Escobar-Sánchez, M.L.; López-Ortiz, M.; Hernández-Rodríguez, M.; Regla, I. Identification of (1S, 4S)-2, 5-diazabicyclo [2.2.1] heptane-dithiocarbamate-nitrostyrene hybrid as potent antiproliferative and apoptotic inducing agent against cervical cancer cell lines. *Eur. J. Med. Chem.* **2018**, *146*, 621–635. [[CrossRef](#)] [[PubMed](#)]
3. Qin, Y.; Liu, S.; Xing, R.; Yu, H.; Li, K.; Meng, X.; Li, R.; Li, P. Synthesis and characterization of dithiocarbamate chitosan derivatives with enhanced antifungal activity. *Carbohydr. Polym.* **2012**, *89*, 388–393. [[CrossRef](#)]

4. Oliveira, J.W.D.F.; Rocha, H.A.O.; de Medeiros, W.M.T.Q.; Silva, M.S. Application of dithiocarbamates as potential new antitrypanosomatids-drugs: Approach chemistry, functional and biological. *Molecules* **2019**, *24*, 2806. [[CrossRef](#)]
5. Song, Z.; Zhou, Y.; Zhang, W.; Zhan, L.; Yu, Y.; Chen, Y.; Jia, W.; Liu, Z.; Qian, J.; Zhang, Y.; et al. Base promoted synthesis of novel indole-dithiocarbamate compounds as potential anti-inflammatory therapeutic agents for treatment of acute lung injury. *Eur. J. Med. Chem.* **2019**, *171*, 54–65. [[CrossRef](#)] [[PubMed](#)]
6. Pal, D.S.; Mondal, D.K.; Datta, R. Identification of metal dithiocarbamates as a novel class of antileishmanial agents. *Antimicrob. Agents Chemother.* **2015**, *59*, 2144–2152. [[CrossRef](#)]
7. Bai, L.; Hu, H.; Fu, W.; Wan, J.; Cheng, X.; Zhuge, L.; Xiong, L.; Chen, Q. Synthesis of a novel silica-supported dithiocarbamate adsorbent and its properties for the removal of heavy metal ions. *J. Hazard. Mater.* **2011**, *195*, 261–275. [[CrossRef](#)]
8. Mujawar, S.; Utture, S.C.; Fonseca, E.; Matarrita, J.; Banerjee, K. Validation of a GC–MS method for the estimation of dithiocarbamate fungicide residues and safety evaluation of mancozeb in fruits and vegetables. *Food Chem.* **2014**, *150*, 175–181. [[CrossRef](#)] [[PubMed](#)]
9. Rohit, J.V.; Basu, H.; Singhal, R.K.; Kailasa, S.K. Development of p-nitroaniline dithiocarbamate capped gold nanoparticles-based microvolume UV–vis spectrometric method for facile and selective detection of quinalphos insecticide in environmental samples. *Sens. Actuators B Chem.* **2016**, *237*, 826–835. [[CrossRef](#)]
10. Liu, B.; Wang, D.; Yu, G.; Meng, X. Removal of F<sup>−</sup> from aqueous solution using Zr (IV) impregnated dithiocarbamate modified chitosan beads. *J. Chem. Eng.* **2013**, *228*, 224–231. [[CrossRef](#)]
11. Alberts, B.; Johnson, A.; Lewis, J.; Raff, M.; Roberts, K.; Walter, P. *Molecular Biology of the Cell*; Garland Science: New York, NY, USA, 2014.
12. Aslanli, A.; Domnin, M.; Stepanov, N.; Efremenko, E. Synergistic Antimicrobial Action of Lactoferrin-Derived Peptides and Quorum Quenching Enzymes. *Int. J. Mol. Sci.* **2023**, *24*, 3566. [[CrossRef](#)] [[PubMed](#)]
13. Maiuolo, L.; Olivito, F.; Algieri, V.; Costanzo, P.; Jiritano, A.; Tallarida, M.A.; Tursi, A.; Sposato, C.; Feo, A.; De Nino, A. Synthesis, Characterization and Mechanical Properties of Novel Bio-Based Polyurethane Foams Using Cellulose-Derived Polyol for Chain Extension and Cellulose Citrate as a Thickener Additive. *Polymers* **2021**, *13*, 2802. [[CrossRef](#)]
14. Cheekatla, S.R.; Thurakkal, L.; Jose, A.; Barik, D.; Porel, M. Aza-Oxa-Triazole Based Macrocycles with Tuneable Properties: Design, Synthesis, and Bioactivity. *Molecules* **2022**, *27*, 3409. [[CrossRef](#)]
15. Thurakkal, L.; Nanjan, P.; Porel, M. Design, synthesis and bioactive properties of a class of macrocycles with tuneable functional groups and ring size. *Sci. Rep.* **2022**, *12*, 4815. [[CrossRef](#)] [[PubMed](#)]
16. Reith, M.A.; De Franceschi, L.; Soete, M.; Badi, N.; Aksakal, R.; Du Prez, F.E. Sequence-Defined Mikto-Arm Star-Shaped Molecules. *J. Am. Chem. Soc.* **2022**, *144*, 7236–7244. [[CrossRef](#)]
17. Kanibolotsky, A.L.; Laurand, N.; Dawson, M.D.; Turnbull, G.A.; Samuel, I.D.W.; Skabara, P.J. Design of Linear and Star-Shaped Macromolecular Organic Semiconductors for Photonic Applications. *Acc. Chem. Res.* **2019**, *52*, 1665–1674. [[CrossRef](#)]
18. Yag, D.P.; Oo, M.N.N.L.; Deen, G.R.; Li, Z.; Loh, X.J. Nano-Star-Shaped Polymers for Drug Delivery Applications. *Macromol. Rapid Commun.* **2017**, *38*, 1700410.
19. Kanibolotsky, A.L.; Perepichka, I.F.; Skabara, P.J. Star-Shaped  $\pi$ -Conjugated Oligomers and Their Applications in Organic Electronics and Photonics. *Chem. Soc. Rev.* **2010**, *39*, 2695–2728. [[CrossRef](#)]
20. Biela, T.; Duda, A.; Penczek, S. Enhanced Melt Stability of Star-Shaped Stereocomplexes as Compared with Linear Stereocomplexes. *Molecules* **2006**, *39*, 3710–3713. [[CrossRef](#)]
21. Jose, A.; Porel, M. Backbone and Side Chain-Linker Tunability among Dithiocarbamate, Ester and Amide in Sequence-Defined Oligomers: Synthesis and Structure-Property-Function Relationship. *Polym. Chem.* **2022**, *13*, 2450–2458. [[CrossRef](#)]
22. Olivito, F.; Amodio, N.; Di Gioia, M.L.; Nardi, M.; Oliverio, M.; Juli, G.; Tassone, P.; Procopio, A. Synthesis and preliminary evaluation of the anti-cancer activity on A549 lung cancer cells of a series of unsaturated disulfides. *Med. Chem. Commun.* **2019**, *10*, 116. [[CrossRef](#)]
23. Altintop, M.D.; Özdemir, A.; Kaplancikli, Z.A.; Turan-Zitouni, G.; Temel, H.E.; Çiftçi, G.A. Synthesis and biological evaluation of some pyrazoline derivatives bearing a dithiocarbamate moiety as new cholinesterase inhibitors. *Arch. Pharm.* **2013**, *346*, 189–199. [[CrossRef](#)] [[PubMed](#)]
24. El-Sagheer, A.H.; Sanzone, A.P.; Gao, R.; Tavassoli, A.; Brown, T. Biocompatible artificial DNA linker that is read through by DNA polymerases and is functional in Escherichia coli. *Proc. Natl. Acad. Sci. USA* **2011**, *108*, 11338–11343. [[CrossRef](#)]
25. Zhou, C.H.; Wang, Y. Recent researches in triazole compounds as medicinal drugs. *Curr. Med. Chem.* **2012**, *19*, 239–280. [[CrossRef](#)]
26. Shinde, S.D.; Sakla, A.P.; Shankaraiah, N. An Insight into Medicinal Attributes of Dithiocarbamates: Bird’s Eye View. *Bioorg. Chem.* **2020**, *105*, 104346–104364. [[CrossRef](#)]
27. Adokoh, C.K. Therapeutic Potential of Dithiocarbamate Supported Gold Compounds. *RSC Adv.* **2020**, *10*, 2975–2988. [[CrossRef](#)]
28. Ajiboye, T.O.; Ajiboye, T.T.; Marzouki, R.; Onwudiwe, D.C. The Versatility in the Applications of Dithiocarbamates. *Int. J. Mol. Sci.* **2022**, *23*, 1317. [[CrossRef](#)] [[PubMed](#)]
29. Thurakkal, L.; Cheekatla, S.R.; Porel, M. Superfast Capture of Iodine from Air, Water, and Organic Solvent by Potential Dithiocarbamate-Based Organic Polymer. *Int. J. Mol. Sci.* **2023**, *24*, 1466. [[CrossRef](#)] [[PubMed](#)]
30. Crnogorac, G.; Schwack, W. Residue Analysis of Dithiocarbamate Fungicides. *TrAC Trends Anal. Chem.* **2009**, *28*, 40–50. [[CrossRef](#)]

31. Saiyed, T.A.; Adeyemi, J.O.; Saibu, G.M.; Singh, M.; Oyedeji, A.O.; Hosten, E.C.; Onwudiwe, D.C. Bipyridine Adducts of Zn (II) and Ni (II) Bis (N-Methyl-N-Phenyl Dithiocarbamate): Synthesis, Characterization, and Biological Applications. *J. Mol. Struct.* **2023**, *1274*, 134335. [[CrossRef](#)]
32. Liu, C.; Liu, Z.; Fang, Y.; Liao, Z.; Zhang, Z.; Meng, L.; Zhang, Z. Exposure to Dithiocarbamate Fungicide Maneb in Vitro and in Vivo: Neuronal Apoptosis and Underlying Mechanisms. *Environ. Int.* **2023**, *171*, 107696. [[CrossRef](#)]
33. Mufhandu, H.T.; Obisesan, O.S.; Ajiboye, T.O.; Mhlanga, S.D.; Onwudiwe, D.C. Antiviral Potential of Selected N -Methyl- N -Phenyl Dithiocarbamate Complexes against Human Immunodeficiency Virus (HIV). *Microbiol. Res.* **2023**, *14*, 355–370. [[CrossRef](#)]
34. Zhou, H.; Gao, C.; Wang, L. Enhancement of the Thermoelectric Performance. *J. Mater. Chem. C.* **2020**, *14*, 7096–7103. [[CrossRef](#)]
35. Anthwal, A.; Singh, K.; Rawat, M.S.M.; Tyagi, A.K.; Aggarwal, B.B.; Rawat, D.S. C5-curcuminoid-dithiocarbamate based molecular hybrids: Synthesis and anti-inflammatory and anti-cancer activity evaluation. *RSC Adv.* **2014**, *4*, 28756–28764. [[CrossRef](#)]
36. Yeo, C.I.; Tiekink, E.R.T. Insights into the Antimicrobial Potential of Dithiocarbamate Anions and Metal-Based Species. *Inorganics* **2021**, *9*, 48. [[CrossRef](#)]
37. Kharb, R.; Sharma, P.C.; Yar, M.S. Pharmacological Significance of Triazole Scaffold. *J. Enzyme Inhib. Med. Chem.* **2011**, *26*, 1–21.
38. Miller, J.; Brooks, E.; Libeu, C.P.; Legleiter, J.; Hatters, D.; Curtis, J.; Cheung, K.; Krishnan, P.; Mitra, S.; Widjaja, K.; et al. Identifying Polyglutamine Protein Species in Situ That Best Predict Neurodegeneration. *Nat. Publ. Gr.* **2012**, *8*, 925–934. [[CrossRef](#)]
39. Peyton, L.R.; Gallagher, S.; Hashemzadeh, M. Triazole antifungals: A review. *Drugs Today* **2015**, *51*, 705–718. [[CrossRef](#)]
40. Epple, S.; Modi, A.; Baker, Y.R.; We, E.; Traor, D.; Wanat, P.; Tyburn, A.E.S.; Shivalingam, A.; Taemaitree, L.; El-sagheer, A.H.; et al. A New 1,5-Disubstituted Triazole DNA Backbone Mimic with Enhanced Polymerase Compatibility. *J. Am. Chem. Soc.* **2021**, *143*, 16293–16301. [[CrossRef](#)] [[PubMed](#)]
41. Atasoy, S.; Ulusoy, N. Activity Studies of New and Highly Selective 1, 2, 3-Triazole Substituted 4-Hydroxybenzohydrazide Derivatives. *J. Mol. Struct.* **2023**, *1283*, 135247–135263.
42. Elmorsy, M.R.; Latif, E.A.; Gaffer, H.E.; Mahmoud, S.E.; Fadda, A.A. Anticancer Evaluation and Molecular Docking of New Pyridopyrazolo-Triazine and Pyridopyrazolo-Triazole Derivatives. *Sci. Rep.* **2023**, *13*, 2782. [[CrossRef](#)]
43. Basar, A.; Hosen, F.; Kumar, B.; Hasan, R.; Shamim, S.M.; Bhuyian, T. Informatics in Medicine Unlocked Identification of Drug and Protein-Protein Interaction Network among Stress and Depression: A Bioinformatics Approach. *Inform. Med. Unlocked* **2023**, *37*, 101174–101184. [[CrossRef](#)]
44. Jose, A.; Porel, M. Chemistry Probing the Interactions of Dansyl Appended Sequence-Defined Oligomers with Serum Albumins: Effect of Functionality, Hydrophobicity, and Architecture. *J. Photochem. Photobiol. A Chem.* **2023**, *439*, 114640–114652.
45. Sun, H.; Wang, J. Novel Perspective for Protein—Drug Interaction Analysis: Atomic Force Microscope. *Analyst* **2023**, *16*, 454–474. [[CrossRef](#)]
46. Mizutani, S.; Pauwels, E.; Stoven, V.; Goto, S.; Yamanishi, Y. Relating drug–protein interaction network with drug side effects. *Bioinformatics* **2012**, *28*, i522–i528. [[CrossRef](#)] [[PubMed](#)]
47. Trott, O.; Olson, A.J. AutoDock Vina: Improving the speed and accuracy of docking with a new scoring function, efficient optimization, and multithreading. *J. Comput. Chem.* **2010**, *31*, 455–461. [[CrossRef](#)] [[PubMed](#)]
48. Morris, G.M.; Huey, R.; Lindstrom, W.; Sanner, M.F.; Belew, R.K.; Goodsell, D.S.; Olson, A.J. AutoDock4 and AutoDockTools4: Automated docking with selective receptor flexibility. *J. Comput. Chem.* **2009**, *30*, 2785–2791. [[CrossRef](#)]
49. Ranjith, D. Molecular Docking Studies of Aloe Vera for Their Potential Antibacterial Activity Using Argus Lab 4.0.1. *Pharma Innov. J.* **2019**, *8*, 481–487.
50. Biovia, D.S. *Discovery Visualizer Studio*; Dassault Systèmes: San Diego, CA, USA, 2019.
51. Xu, J.; Avellan, A.; Li, H.; Liu, X.; Noël, V.; Lou, Z.; Wang, Y.; Kaegi, R.; Henkelman, G.; Lowry, G.V. Sulfur loading and speciation control the hydrophobicity, electron transfer, reactivity, and selectivity of sulfidized nanoscale zerovalent iron. *Adv. Mater.* **2020**, *32*, 1906910–1906920. [[CrossRef](#)]
52. Gakamskya, D.; Gakamskyb, A. Intrinsic fluorescence of proteins as a medical diagnostic tool. *Int. J. Spectrosc.* **2017**, *29*, 6–10.

**Disclaimer/Publisher’s Note:** The statements, opinions and data contained in all publications are solely those of the individual author(s) and contributor(s) and not of MDPI and/or the editor(s). MDPI and/or the editor(s) disclaim responsibility for any injury to people or property resulting from any ideas, methods, instructions or products referred to in the content.